EDGE ARTICLE

Check for updates

Spin multiplicity effects in doublet *versus* singlet emission: the photophysical consequences of a single electron†

Caleb M. Wehrmann, [iD] ‡ Muhammad Imran, [iD] ‡ Craig Pointer, [iD] Lisa A. Fredin, [iD] * Elizabeth R. Young [iD] * and Mark S. Chen [iD] *

Ambient-stable fluorescent radicals have recently emerged as promising luminescent materials; however, tailoring their properties has been difficult due to the limited photophysical understanding of open-shell organic systems. Here we report the experimental and computational analysis of a redox pair of π-conjugated fluorescent molecules that differ by one electron. A π-dication (**DC**) and π-radical cation (**RC**) demonstrate different absorption spectra, but similar red emission ($\lambda_{emiss,max} = \sim630$ nm), excitation maxima ($\lambda_{exc,max} = \sim530$ nm), fluorescence lifetimes (1–10 ns), and even excited-state (non-emissive) lifetimes when measured by transient absorption spectroscopy. Despite their experimental similarities, time-dependent density functional theory (TDDFT) studies reveal that **DC** and **RC** emission mechanisms are distinct and rely on different electronic transitions. Excited-state reorganization occurs by hole relaxation in singlet **DC**, while doublet **RC** undergoes a Jahn-Teller distortion by bending its π-backbone in order to facilitate spin-pairing between singly occupied molecular orbitals. This relationship between the excited-state dynamics of **RC** and its π-backbone geometry illustrates a potential strategy for developing π-conjugated radicals with new emission properties. Additionally, by comparing TDDFT and CIS (configuration interaction singles) excitations, we show that unrestricted TDDFT accurately reproduces experimental absorption spectra and provides an opportunity to examine the relaxed excited-state properties of large open-shell molecules like **RC**.

Introduction

Photoluminescence (PL) is the process in which a photo-generated excited state relaxes *via* emission of a photon.[1] Since many photochemical applications are dependent on absorption or emission-related phenomena (or both), investigations that clarify the photophysical mechanisms of PL and related processes are critical to the development of photoactive materials for chemical sensing,[2] photocatalysis,[3] and light-emitting diodes.[4]

All PL is classified as either fluorescence or phosphorescence based on whether emission occurs by radiative decay from an excited state with spin multiplicity that is the same as or higher than the ground state, respectively. Most organic compounds possess an even number of electrons resulting in all paired spins (*i.e.* they are closed-shell molecules). Consequently, fluorescence derives from singlet excited states (S_n), while phosphorescence derives from triplet excited states (T_n). Recently, however,

photophysical phenomena that derive from excitation of doublet ground states (*i.e.* an odd number of electrons that leads to one unpaired spin) have begun to be considered with reports of emissive, air-stable, organic radicals (*i.e.* open shell molecules) that demonstrate short luminescence lifetimes (<10 ns).[5] Fluorescence and phosphorescence in monoradicals instead derive from doublet (D_n) or quartet (Q_n) excited states, respectively.

Spin multiplicity effects have been studied in other luminescent compounds, particularly for metal complexes.[6] However, such an investigation has been difficult with organic molecules because it requires a single electron redox pair that shows sufficient stability and photoluminescence in both closed- and open-shell oxidation states.

Due to challenges in achieving persistence in air, nearly all examples of ambient stable, emissive organic radicals stabilize unpaired spin using a triarylmethyl motif.[5,7] While these fluorescent radicals have already shown utility in various applications, their photophysical properties have yet to be compared with their redox-related anion or cation.

Herein we report a recently discovered phenalenyl-based,[8] stable π-radical cation (**RC**) that shares red fluorescence with its dicationic, closed-shell precursor (**DC**) (Fig. 1).[9] Despite their electronic differences, both species show remarkably similar emission, solvent-dependent behaviours, and even excited-state

Department of Chemistry, Lehigh University, Bethlehem, PA 18015, USA. E-mail: mschen@lehigh.edu; ery317@lehigh.edu; laf218@lehigh.edu

† Electronic supplementary information (ESI) available. See DOI: 10.1039/d0sc04211k
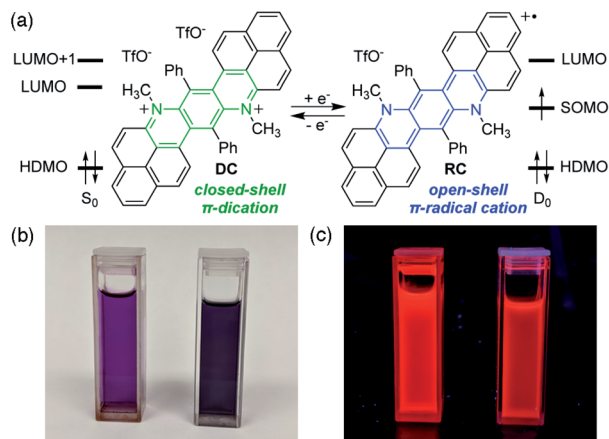
‡ C. M. W. and M. I. contributed equally to this work.

Fig. 1 Structure of dication (DC) and π-radical cation (RC) with their corresponding frontier molecular orbitals (a), and photographs of each species under illumination by white light (b) and ultraviolet (360 nm) light (c). LUMO = lowest unoccupied molecular orbital, HDMO = highest doubly occupied molecular orbital, SOMO = singly occupied molecular orbital.
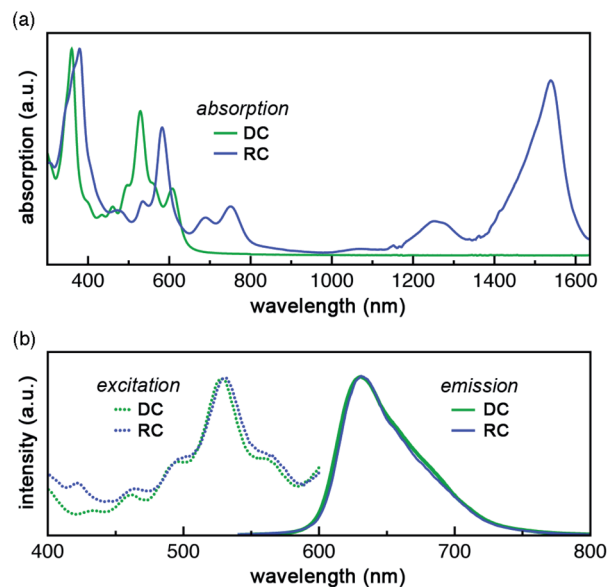

Fig. 2 (a) Absorption spectra of DC (green) and RC (blue) that highlight their overall differences in electronic structure. (b) Excitation (dotted) and emission (solid) spectra of DC (green) and RC (blue) highlight the near-identical excitation and emission behaviours. The DC and RC spectra overlap so closely that their spectra are difficult to differentiate. Spectra are recorded in ~3 μM solutions of DC or RC in acetonitrile. Excitation spectra are recorded with emission at 630 nm. Emission spectra are recorded with excitation at 534 nm. The absorption and emission spectra are normalized to aid in comparison.

dynamics. Specifically, although different electronic transitions are responsible for emission in DC and RC, the observed wavelengths are near-identical between species because of significant structural and electronic reorganization in excited RC. This reorganization arises from spin-(un)pairing in the singly occupied molecular orbitals of RC, which is a key distinguishing feature between the electronic structures of doublet and singlet excited states. Disentanglement of the different excited-state manifolds of this single electron redox pair of emissive π-conjugated organics is accomplished through the powerful combination of steady-state and time-resolved spectroscopies and quantum mechanical calculations.

Results and discussion

Absorption and photoluminescence

DC and RC share two strong absorption bands at 530–540 nm and 590–610 nm (in acetonitrile) that arise from electronic transitions originating from the doubly occupied molecular orbital manifold into the unoccupied molecular orbital manifold. Additionally, RC shows several longer wavelength features (>650 nm) that are associated with promotion of the unpaired electron (Fig. 2a, *vide infra*).[9]

Despite these differences in absorption features, DC and RC share a surprisingly near-identical red emission ($\lambda_{emiss,max}$ = 632 nm and $\lambda_{emiss,max}$ = 630 nm, respectively, solid lines Fig. 2b) upon irradiation at wavelengths higher in energy than the highest doubly occupied molecular orbital (HDMO) to lowest unoccupied molecular orbital (LUMO) energy gap (*i.e.* λ_{exc} < 650 nm, dotted lines). The highest photoluminescence (PL) intensity was achieved with excitation wavelengths of ~530 nm. To identify what electronic transitions are responsible for PL, we measured the PL excitation (PLE) spectrum that corresponds to the $\lambda_{emiss,max}$ for both DC and RC. The maximum PLE intensity for DC is 530 nm, as shown in Fig. 2b (dotted green line), and the

maximum PLE intensity for RC is 534 nm (dotted blue line Fig. 2b and S3†). The PL lifetimes of DC and RC are measured to be 1.42 ns and 3.40 ns, respectively, which are typical for organic fluorescence. Although RC shows several lower energy absorption peaks, irradiation at longer wavelengths (λ_{exc} > 650 nm) does not result in emission wavelengths shorter than 1350 nm, likely due to competing non-radiative decay pathways (Table S3†). Moreover, excitation of RC at varying wavelengths (λ_{exc}) leads to only one emission peak, which suggests that there is only one emissive excited state (Fig. S3†).

Relative photoluminescence quantum yields (PLQY, Φ_{PL}) of DC and RC were determined by calibration to known standards and found to be 11.8% and 5.8%, respectively, which are values within the range of other fluorescent radicals.[5,7] In combination with PL lifetimes (τ_{PL}), these PLQY values enable us to calculate radiative (k_r) and non-radiative (k_{nr}) decay rates (eqn (1) and (2)). For DC, $k_r = 8.3 \times 10^7$ s^{-1} and $k_{nr} = 62.1 \times 10^7$ s^{-1}, and for RC, $k_r = 1.7 \times 10^7$ s^{-1} and $k_{nr} = 27.7 \times 10^7$ s^{-1}. Interestingly, despite the clear difference in quantum yields, DC and RC show near-identical rates of radiative and non-radiative decay.

$$\tau_{PL} = \frac{1}{k_r + k_{nr}} \tag{1}$$

$$\Phi_{PL} = \frac{k_r}{k_r + k_{nr}} \tag{2}$$

The photochemical similarities between DC and RC are extraordinary, and might even lead one to suspect that they

result from the generation of a common species upon irradiation. However, absorption spectra recorded before and after each PL measurement (Fig. S5†) verified that distinct samples of **DC** and **RC** remained homogeneous and did not decompose. The near-identical PLE ($\lambda_{exc,max}$) and PL ($\lambda_{emiss,max}$) maxima, suggest that fluorescence in both compounds must rely on very similar orbital transitions, which can only arise if there are some similarities in the electronic structure of **DC** and **RC** (*vide infra* and Fig. S18†). Since the emission of **DC** is redshifted from all of its absorption bands, we can infer that emission originates from the lowest singlet excited state (S_1). In contrast, the emission of **RC** occurs at shorter wavelengths than multiple absorption bands, which indicates that **RC** violates Kasha's rule.[10]

Solvent effects

Changes to solvent polarity lead to alterations in steady-state characteristics that provide insight to the nature of these transitions. Spectroscopic characterization of **DC** was carried out in acetone and ethyl acetate, in addition to acetonitrile (ACN) reported above. **DC** in acetone produces similar spectra to those obtained in ACN; however, the PLQY increases from 11.8% up to 16.2% (Table 1). Solvation in ethyl acetate leads to even further PLQY increases (26.0%), a longer PL lifetime (1.96 ns), and a redshifted emission (λ_{max} = 642 nm) when compared to ACN. These data are indicative of a decrease in the dipole moment of **DC** upon excitation, such that the excited state is more stabilized by less polar solvents.

Due to **RC** being soluble in dichloromethane (DCM), but not in acetone or ethyl acetate, the solvent polarity was varied for **RC** by using mixtures of ACN and DCM. A solvent trend is less apparent with **RC** because the solvent mixtures (Table 1) do not show intermediate values. Instead solvent mixtures of **RC** produce PLQYs and PL lifetimes greater than either ACN or DCM alone. **RC** in neat DCM displays a PLQY of 9.1% and shows only a small increase in PL lifetime compared to ACN.

Transient absorption (TA) spectroscopy

To understand their excited-state evolution, **DC** and **RC** were analysed by TA spectroscopy in ACN from picosecond to
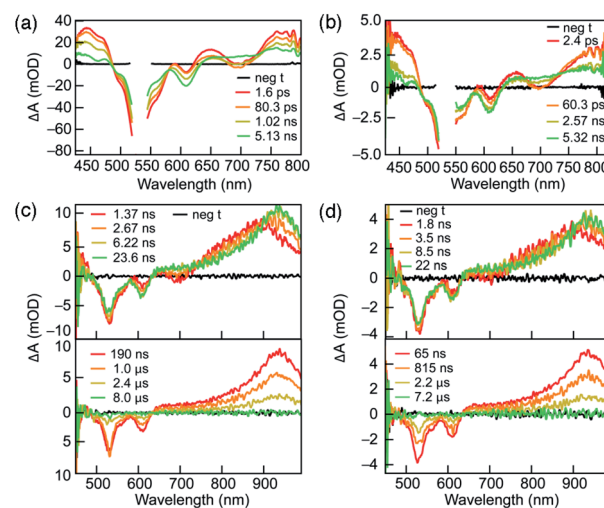

Fig. 3 Transient absorption spectra of **DC** (a and c) and **RC** (b and d) in acetonitrile. (a and b) show kinetics from femtosecond TA spectra from 0 to 5.5 ns. (c and d) show nanosecond TA spectra over a range of time delays. Dilute solutions of **DC** and **RC** were prepared so that the absorption at the excitation wavelength (λ_{exc} = 530 nm) is approximately 0.5 AU. Gaps in the spectra (a and b) around 530 nm correspond to removal of scatter laser excitation light. Note that the picosecond TAS (a and b) have different wavelength ranges than the microsecond TAS (c and d) due to the white light probe sources for each experiment.

microsecond time ranges (Fig. 3). Absorption spectra recorded before and after each TA experiment were found to be identical, which verified that neither compound experienced photoinduced decomposition (Fig. S5†). Both compounds demonstrate near-identical TA features that, like their similarities in PL excitation and emission, arise from similar ground-state electronic structures of **DC** and **RC** (Fig. S16–S18,† *vide infra*).

Similar TA spectra are not expected between related redox species; however, the significant delocalization of charge and spin in both compounds lead to negligible differences in their electronic structures. These common TA features appear to result from comparable relative energy level spacings between the higher unoccupied molecular orbitals (*vide infra* and Fig. S18†) in **DC** and **RC** that produce similar induced

Table 1 Steady-state and time-resolved photophysical characterization of **DC** and **RC** in various solvent conditions. Standard deviations are reported in parentheses

Solvent	Dielectric constant (F m^{-1})	Exc λ_{max} (nm)	PL λ_{max} (nm)	PL lifetime (ns)	PLQY (%)	k_r (10^7 s^{-1})	k_{nr} (10^7 s^{-1})	τ_1 (ps)	τ_2 (ns)	τ_3 (µs)
π-dication (DC)										
ACN	37.5	530	632	1.42 (0.02)	11.8 (0.7)	8.3	62.1	76 (12)	2.1 (0.3)	1.8 (0.1)
Acetone	20.7	529	632	1.52 (0.01)	16.2 (3.0)	10.7	55.1	59 (6)	2.1 (0.3)	1.7 (0.1)
Ethyl acetate	6.02	532	642	1.96 (0.08)	26.0 (1.4)	13.3	37.7	114 (38)	2.3 (0.3)	2.6 (0.3)
π-radical cation (RC)										
ACN	37.5	534	630	3.40 (0.15)	5.8 (0.6)	1.7	27.7	106 (25)	2.9 (0.1)	1.8 (0.2)
ACN : DCM (1 : 1)	—	534	632	4.23 (0.1)	11.8 (1.9)	2.8	20.9	15.4 (0.7)	3.0 (0.3)	2.4 (0.3)
ACN : DCM (1 : 2)	—	536	635	3.96 (0.12)	10.1 (0.6)	2.6	22.7	10.8 (0.1)	3.1 (0.4)	2.4 (0.2)
DCM	8.93	537	634	3.32 (0.02)	9.1 (0.2)	2.7	27.4	11 (1.0)	2.8 (0.3)	3.4 (0.5)

absorptions. Therefore, it is difficult to distinguish the transient absorption spectra of **RC** from **DC** in the visible absorption region. The α-SUMO-related for transitions for **RC** correspond to lower energy absorption features that lie outside the detection window of our TA analysis (>800 nm). The visible TA spectra show negative ΔA centred at ~530 nm and ~610 nm corresponds to ground-state bleaching of both **DC** and **RC**. The appearance of positive ΔA peaks, convolved with the ground-state bleach, are centred at 450 nm, 650 nm, and > 750 nm and represent the formation of the initial excited state. The excited-state growths at wavelengths greater than 750 nm obscure the expected ground-state bleach of the **RC** at ~750 nm due to the convolution of the two signals. The initial excited state decays to form an intermediate species with a very broad positive signal between 650 and 850 nm (Fig. 3a and b). During the first 25 nanoseconds (Fig. 3c and d, top tile), the signal > 700 nm continues to slightly redshift ending up as a peak at ~950 nm (Fig. 3c and d). Concomitant decay of the 950 nm peak and recovery of the ground-state bleach is observed in less than 10 μs and corresponds with return to the ground state.

The solvent-dependence of **DC** and **RC** excited-state evolution were evaluated for **DC** in ethyl acetate and acetone, and for **RC** in DCM and varying ratios of ACN : DCM (1 : 1 or 1 : 2), along with ACN (*vide supra*) (Fig. S6 and S7†). The TA spectra obtained for each solvent condition show features very similar to those observed in acetonitrile, thereby suggesting that the formation of similar excited state species occurs independent of solvent.

Due to the complicated spectral evolution observed for **DC** and **RC**, global analysis fitting was performed to extract individual lifetime components of the spectral evolution. Each component is referred to as a decay-associated difference spectrum (DADS). Global analysis fitting for **DC** and **RC** yielded three lifetimes, each associated with a separate DADS, and each decaying at different timescales: ps, ns, or μs ranges (Table 1, Fig. S8 and S9†). The shortest lifetime (τ_1) is assigned to rapid vibrational relaxation and transition to a lower energy excited state. For **DC**, τ_1 is not affected by solvent polarity; however, a trend is present in the DADS of **RC**. Since the τ_1 values for the ACN : DCM solvent mixtures (Table 1) are more similar to DCM, we postulate that these convoluted solvent trends at shorter time scales are due to **RC** possessing a preferential solvent shell of DCM even when ACN is present.

The lifetimes of the second DADS component (τ_2) for **DC** and **RC** are ~2 ns and ~3 ns, respectively, with no distinguishable trend with solvent. The τ_2 component is assigned to radiative decay responsible for the observed fluorescence, based on the agreement between τ_2 lifetimes measured by TA and time-resolved PL lifetimes.

The lifetimes of the third and longest-lived DADS component (τ_3) fall within 1–4 μs for **DC** and **RC**. Lifetimes of this order of magnitude often result from spin or symmetry forbidden transitions back to the ground state. We propose that the long-lived **DC** species (τ_3) represents an excited triplet state based on its decay lifetime and the similarity of its absorption (λ_{max} ~950 nm) with the calculated energy differences between the first (T_1) and higher (T_n) triplet excited states (Table S8†). This assignment is supported by the fluorescence detection of singlet oxygen when **DC** is irradiated (530 nm) in the presence of molecular oxygen, since oxygen sensitization commonly proceeds by energy transfer from excited triplets (Fig. S4†).[11] The long-lived lifetime of the doublet **RC** might, by analogy, be assumed to result from relaxation from a quartet that forms during intersystem crossing from the doublet excited state. However, the calculated quartet (Q_1, Table S1†) is isoenergetic with the excited-state, which suggests that there is no driving force for intersystem crossing and thus the long lifetime likely results from doublet symmetry forbidden transitions (*vide infra*).

The lifetime of the longest-lived species (τ_3) increases with decreasing solvent dipole moment. For **DC**, ethyl acetate produces the longest lifetime (2.6 μs) compared to acetone or ACN (Table 1). For **RC**, DCM yields the longest lifetime (3.4 μs), ACN : DCM mixtures show intermediate lifetimes (2.4 μs), and ACN leads to the shortest lifetime of 1.8 μs. These trends between solvent polarity and τ_3 lifetimes support the formation of excited states with a lower dipole moment than the ground states. For such species, less polar solvents are more effective for stabilization of the excited state, thereby promoting longer τ_3 lifetimes.

Quantum mechanical calculations

Clarification of the emission mechanisms in **DC** and **RC** was achieved through quantum chemical calculations. Structure optimizations were performed in Gaussian D.01 (ref. 12) using the hybrid B3LYP functional and a double-ζ basis set with polarization and dispersion [6-31g+(d,p)] to best model the delocalized π-networks. An ACN polarization continuum model of solvation[13] was applied to allow for more charge localization, and GD3 empirical dispersion was used to account for the diffuse π-bonds. A closed-shell restricted formalism was used to optimize the singlet ground state of **DC**, whereas an unrestricted formalism was necessary to optimize the doublet ground state of **RC** due to its unpaired electron. While a restricted formalism forces electrons to pair in occupied molecular orbitals in the conventional spin-up–spin-down manner, an unrestricted formalism results in α (spin down) and β (spin up) sets of singly occupied orbitals. Therefore, in **RC** the singly occupied molecular orbital (SOMO) becomes the α-SOMO and each doubly occupied orbital is computed as two (one α and one β) SOMOs, such that the HDMO is the α-SOMO-1 and β-SOMO.

One of the most ubiquitous uses of time-dependent (TD)[14] implementations of DFT is to model the absorption spectra of singlet ground state molecules. However, when it is applied to organic and inorganic systems of higher multiplicity, large spin-contamination leads to errors in orbital transition assignments by as much as 3 eV.[15] In contrast, the configuration interaction (CI) description of orbital overlap between non-singlet orbitals, makes CI singles (CIS) highly effective for predicting absorption spectra and excitation energies, even of higher spin systems. The main limitation for CIS is that it is resource intensive and thus recent implementations of excited state geometry

optimization[16] are still severely limited to small π-conjugated systems. Alternatively, TDDFT is known to effectively optimize excited states of even large systems, making it an attractive method to simulate the photophysical properties of fluorescent radicals. Because most TDDFT implementations presume that ground state orbitals possess singlet multiplicity, it is important to check if excitations between the highly delocalized doublet Kohn-Sham orbitals of **RC** accurately reflect experimental data.[17]

Notably, the ground-state structures of **DC** and **RC** are nearly identical across a range of hybrid functionals, which indicates that the presence (or absence) of one electron does not greatly affect overall bonding and geometry. This structural similarity is probably due to highly delocalized frontier molecular orbitals, which extend throughout the entire π-backbone. The nature of the molecular orbitals of **DC** and **RC** are remarkably similar, despite the splitting of the occupation of orbitals and the addition of an electron in **RC**. The molecular orbitals differ only in energies, but not in their ordering, symmetry, or spacing (Fig. S16 and S17†). For example, the **DC** LUMO is the same π-symmetry as the α-SOMO in **RC**. These unusual similarities between **DC** and **RC** provide an explanation for their near-identical PL and TA spectra (*vide supra*, Fig. S18†). As discussed above, the common TA spectral features of **DC** and **RC** likely originate from their having comparable relative energy levels between higher unoccupied molecular orbitals.

Interestingly, the α-SOMO and β-LUMO energy levels in **RC** differ by much less (0.96 eV) than analogous MOs calculated for the reported triarylmethyl radicals,[5,7] which leads to the low energy transitions seen in the absorption spectra of **RC**. In addition, **DC** and **RC** excitations modeled by CIS and TDDFT with various common functionals[14] are all remarkably similar (Fig. S20 and S21†).

CIS and TDDFT predict very similar absorption for **DC** with only a minor blue shift from the experimental absorption spectra (Fig. 4a, Tables S5–S7, S10–S15†). Similarly, CIS and TDDFT provide similar predictions for **RC** absorption and match experimental excitations in the visible range. However, despite our experimental observation of two near-infrared (NIR) peaks at 1276 and 1565 nm (Fig. 4b), both methods predict only one NIR electronic transition: α-SOMO → α-LUMO at 1170 nm and 1350 nm with CIS/D3-B3LYP and TDDFT/D3-B3LYP, respectively (Tables S16–S18 and S20–S25†). As CIS and TDDFT only calculate electronic transitions, we can be relatively certain that only one electronic transition occurs in this region. Considering that the two experimental NIR bands differ by the characteristic C=C stretching frequency (1511 cm^{-1}), we can infer that the lower energy peak (1565 nm) is the $0 \rightarrow 0$ vibronic transition of the α-SOMO → α-LUMO excitation, while the higher energy peak (1276 nm) represents the $0 \rightarrow 1$ vibronic transition. Of the methods and hybrid functionals explored, CIS/CAM-B3LYP provided the closest match (1509 nm) to experiment (Table S22†).

CIS and TDDFT proved relatively accurate for calculating the visible transitions across various functionals. The strong agreement between CIS and TDDFT suggests that linear response TDDFT can be used to model the excited states and
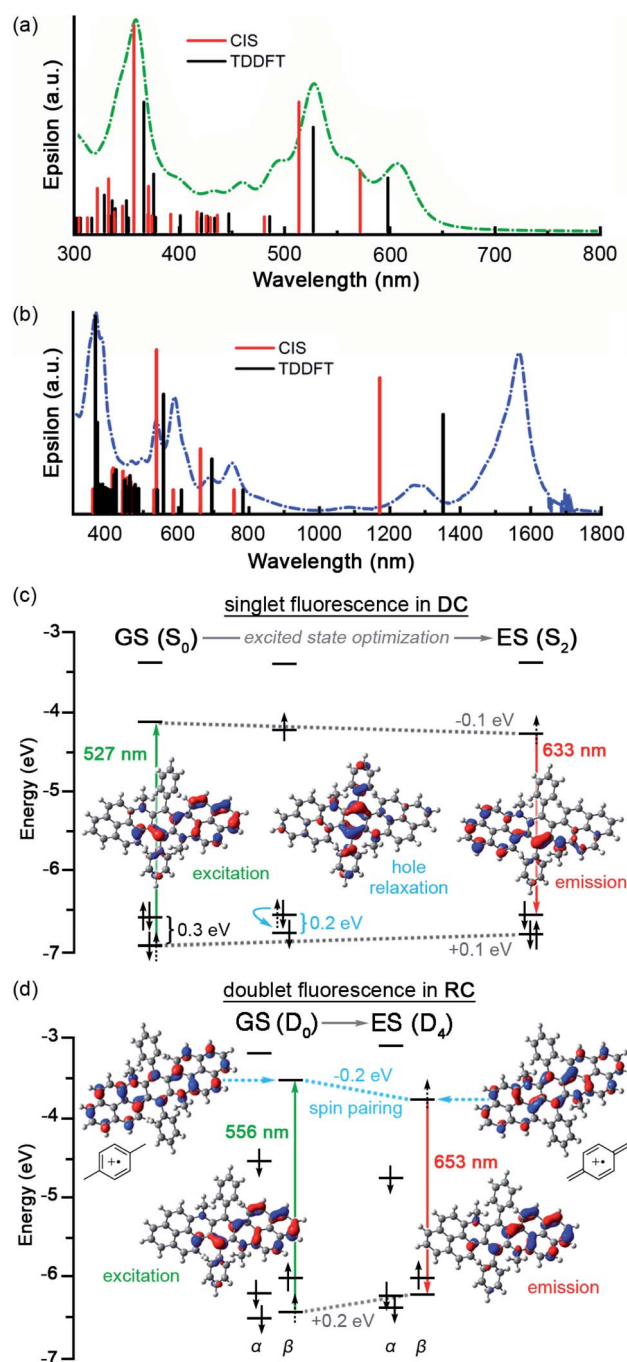

Fig. 4 Comparison of calculated electronic spectra according to TDDFT/D3-B3LYP (black) and CIS/D3-B3LYP (red) calculations for **DC** (a) and **RC** (b). Proposed fluorescence mechanisms for **DC** (c) and **RC** (d) at the D3-B3LYP TDDFT level of theory. Electronic density difference maps are shown for each transition.

resultant excitations not only for the singlet excited state manifold of **DC** but also unrestricted doublet manifold of **RC**.

For **DC**, TDDFT/D3-B3LYP assigns the two lowest energy excitations (599 and 527 nm) to HDMO → LUMO and HDMO-1 → LUMO, respectively. The S$_2$ excited state, which results when an electron is promoted from HDMO-1 to LUMO, is identified as the electronic state from which the experimental excited-state

dynamics originate because its calculated transition energy most closely matches the experimental excitation wavelengths (~530 nm). Optimization of the excited state (S_2) leads to barely any conformational change but a significant decrease in dipole moment (2.24 → 2.04 D), which strongly agrees with stabilization of the excited state in less polar solvents (Fig. S12 and S14†). The electronic structure of the optimized excited state (S_2) indicates that at its relaxed geometry S_2 emits via a LUMO → HDMO transition.

These data suggest that fluorescence in **DC** proceeds by excitation (527 nm) from HDMO-1 (−6.90 eV) to LUMO (−4.14 eV) that is followed by rapid hole relaxation (on the S_2 surface near the S_0 geometry). This assignment is based on the HDMO–HDMO-1 contraction that occurs early in the TDDFT optimization path from S_0 to S_2 geometries (Fig. 4c and S14†). The excited state (S_2) then radiatively decays (632 nm) via an electronic transition from LUMO (−4.22 eV) to HDMO (−6.54 eV) that obeys Kasha's rule (Table S9†).

In **RC**, the excitation that best matches the experimental excitation energy (~534 nm) corresponds to a HDMO-1 → LUMO type excitation (β-SOMO-1 → β-LUMO, in the doublet orbitals), too. Optimization of this excited state (D_4) leads to a lower dipole moment (2.95 → 2.70 D), more quinoidal character, and a Jahn-Teller distortion that manifests as greater bending in the π-backbone. As observed in cyclo-paraphenylenes, increased curvature facilitates quinoidization and spin-pairing stabilization.[18,19] In particular, the low lying β-LUMO electron seems to spin-pair with the electron in the α-SOMO, leading to additional stabilization of the newly populated β-LUMO energy level. This effect is highlighted by the greater decrease in α-SOMO and β-LUMO (~0.2 eV) energy levels versus the LUMO (~0.1 eV) in excited **DC** where spin-pairing is not possible. In addition, spin-unpairing between the α-SOMO-2 and β-SOMO-1 leads to significant destabilization (~0.2 eV) of these orbitals (Fig. 4d and S17†).

Therefore, we propose that **RC** fluorescence proceeds by excitation (556 nm) from β-SOMO-1 (−6.43 eV) to β-LUMO (−3.53 eV) to form the D_4 excited state, that upon relaxation to a Jahn-Teller distorted geometry radiatively decays (653 nm) from β-LUMO (−3.74 eV) to β-SOMO-1 (−6.23 eV). The hole relaxation observed in the excited state optimization of **DC** is not present in the D_4 optimization of **RC** (Fig. S15†). We postulate that hole relaxation is absent in **RC** because of the difference in intrinsic charge on the molecule: a photo-generated hole in a dication (**DC**) is hotter than one in a cation (**RC**).

The mixing of spin multiplicities is small for molecules only containing light atoms, and therefore the oscillator strength (orbital overlap) between the different spin states is also small for organic molecules. Despite this, it is well known that many closed-shell organic molecules can phosphoresce from a triplet state. A small population of ISC to the triplet occurs, despite the small overlap, due to an energetic driving force between excited singlet states and the triplet states. These triplets are long-lived due to the spin forbidden nature of the radiative decay back to the singlet surface. In **RC**, the spin–orbit coupling is small and there is no driving force to form a quartet through ISC, either at

the ground-state geometry or to a relaxed Q_1 state (Table S1†). However, there is significant driving force for IC to D_2 and D_1 from the relaxed excited-state (D_4) supporting formation of a long-lived doublet state. For this state to be long-lived the return to the ground-state must be symmetry forbidden.

Photoresponse of the single electron redox pair

From these data, we can construct a full picture of the photophysical behaviour for both species (Fig. 5). For **DC**, initial excitation (530 nm) leads to formation of S_2, which rapidly under-goes internal conversion (76 ps) via hole relaxation to the lowest excited singlet (S_1). The observed red emission (632 nm, 2.1 ns) is the result of radiative decay from S_1 to S_0 so that fluorescence in **DC** follows Kasha's rule. Additionally, **DC** can also undergo intersystem crossing to access an excited triplet state (T_n) that decays more slowly (1.8 μs) to the ground state (S_0).

Regarding **RC**, excitation (534 nm) generates a thermally excited D_4 that relaxes to its lowest vibrational state prior to radiative decay back to D_0 to provide the observed anti-Kasha fluorescence (630 nm, 2.9 ns). Alternatively, relaxation of **RC** can also proceed by internal conversion (106 ps) from D_4 to lower doublet excited states, which is expected to be slow (1.8 μs) since they represent symmetry forbidden transitions with
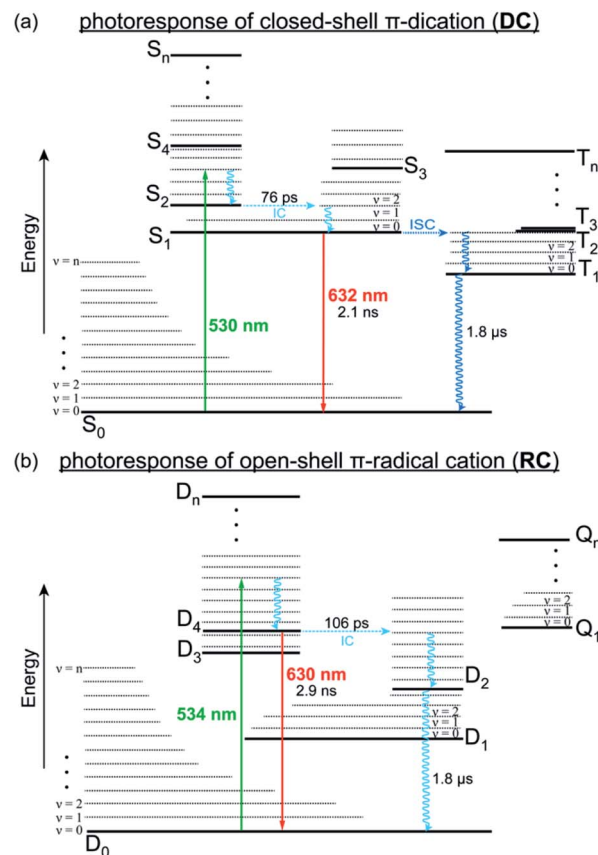

Fig. 5 Jablonski plots that illustrate the relaxation pathways of **DC** (a) and **RC** (b) from their respective excited states, either through radiative (solid lines) or vibronic (wavy lines) transitions.

minimal overlap (Fig. S19†). These lower doublet excited states must instead relax through low frequency ($\nu < 100$ cm^{-1}) vibrational modes, many of which consist of wags along the π-backbone (Table S2†). Generally, π-conjugated molecules are less contorted and therefore only show vibrations along ancillary moieties (Table S4†). The presence of these low energy vibrations however, likely explain why **DC** and **RC** demonstrate $k_{nr} > k_r$ and have relatively low fluorescence quantum yields. They also highlight a structural property that we can look to synthetically modify in order to develop fluorescent radicals with different emission wavelengths and higher quantum efficiencies.

Conclusions

Although the steady-state and time-resolved spectroscopic behaviors of **DC** and **RC** appear identical, TDDFT calculations reveal the consequences of a single unpaired electron. In the absence of an electron, **DC** is an electrophilic dicationic singlet (S_0) that favors hole relaxation prior to emission. Relaxation of the photoexcited state may also proceed through a triplet excited state that is long-lived because of the spin forbidden transition to the ground state. With the addition of an electron, **RC** is a cationic doublet (D_0) that achieves spin-pairing between the excited electron and the α-SOMO in the excited state (D_4) through a Jahn-Teller distortion. The slow decay process in **RC** proceeds through an excited state that shares the same multiplicity (doublet) as the ground state, but is long-lived due to its symmetry forbidden transition. This clarification of doublet excited state dynamics in **RC** is significant since it suggests that tailoring π-backbone flexibility should enable the development of luminescent radicals with new and more efficient emission properties. Furthermore, our computational studies demonstrate the accuracy of unrestricted TDDFT for simulating the excitations and emissions of a large, π-conjugated, open-shell molecule like **RC**, which is representative of a growing class of novel organic materials.

Author contributions

C. M. W. performed the TDDFT calculations, M. I. synthesized the molecules and collected the absorption and photoluminescence data, and C. P. performed the transient absorption spectroscopy. L. A. F., E. R. Y., and M. S. C. designed the experiments and wrote the manuscript.

Conflicts of interest

There are no conflicts to declare.

Acknowledgements

Notes and references

1 N. J. Turro, J. C. Scaiano and V. Ramamurthy, *Modern Molecular Photochemistry of Organic Molecules*, University Science Books, Mill Valley, 2010.

2 (a) H.-W. Liu, L. Chen, C. Xu, Z. Li, H. Zhang, X.-B. Zhang and W. Tan, *Chem. Soc. Rev.*, 2018, **47**, 7140–7180; (b) D. Wu, A. C. Sedgwick, T. Gunnlaugsson, E. U. Akkaya, J. Yoon and T. D. James, *Chem. Soc. Rev.*, 2017, **46**, 7105–7123; (c) H. Zhu, J. Fan and X. Peng, *Acc. Chem. Res.*, 2016, **49**, 2115–2126; (d) M. H. Lee, J. S. Kim and J. L. Sessler, *Chem. Soc. Rev.*, 2014, **44**, 4185–4191.

3 (a) W. Chen, Z. Huang, N. E. S. Tay, B. Giglio, M. Wang, H. Wang, Z. Wu and D. A. Nicewicz, *Science*, 2019, **364**, 1170–1174; (b) N. A. Romero and D. A. Nicewicz, *Chem. Rev.*, 2016, **116**, 10075–10166; (c) N. Corrigan, S. Shanmugam, J. Xu and C. Boyer, *Chem. Soc. Rev.*, 2016, **45**, 6165–6212; (d) J. C. Theriot, C.-H. Lim, H. Yang, M. D. Ryan, C. B. Musgrave and G. M. Miyake, *Science*, 2016, **352**, 1082–1086.

4 (a) T. Chatterjee and K.-T. Wong, *Adv. Opt. Mater.*, 2019, **7**, 1800565; (b) T. Huang, W. Jiang and L. Duan, *J. Mater. Chem. C*, 2018, **6**, 5577–5596; (c) Y. Liu, C. Li, Z. Ren, S. Yan and M. R. Bryce, *Nat. Rev. Mater.*, 2018, **3**, 18020; (d) C. Adachi, *Jpn. J. Appl. Phys.*, 2014, **53**, 060101.

5 (a) Y. Teki, *Chem.–Eur. J.*, 2020, **26**, 980–996; (b) X. Ai, Y. Chen, Y. Feng and F. Li, *Angew. Chem., Int. Ed.*, 2018, **57**, 2869–2873; (c) S. Dong, A. Obolda, Q. Peng, Y. Zhang, S. Marder and F. Li, *Mater. Chem. Front.*, 2017, **1**, 2132–2135; (d) Y. Hattori, T. Kusamoto and H. Nishihara, *Angew. Chem., Int. Ed.*, 2014, **53**, 11845–11848; (e) O. Armet, J. Veciana, C. Rovira, J. Riera, J. Castaner, E. Molins, J. Rius, C. Miravitlles, S. Olivella and J. Brichfeus, *J. Phys. Chem.*, 1987, **91**, 5608–5616.

6 W. Zhang, K. S. Kjær, R. Alonso-Mori, U. Bergmann, M. Chollet, L. A. Fredin, R. G. Hadt, R. W. Hartsock, T. Harlang, T. Kroll, K. Kubicek, H. T. Lemke, H. W. Liang, Y. Liu, M. M. Nielsen, P. Perrson, J. S. Robinson, E. I. Solomon, Z. Sun, D. Sokaras, T. B. van Driel, T.-C. Weng, D. Zhu, K. Wärnmark, V. Sundström and K. J. Gaffney, *Chem. Sci.*, 2017, **8**, 515–523.

7 (a) H. Guo, Q. Peng, X.-K. Chen, Q. Gu, S. Dong, E. W. Evans, A. J. Gillett, X. Ai, M. Zhang, D. Credgington, V. Coropceanu, R. H. Friend, J.-L. Brédas and F. Li, *Nat. Mater.*, 2019, **18**, 977–984; (b) X. Ai, E. W. Evans, S. Dong, A. J. Gillett, H. Guo, Y. Chen, T. J. H. Hele, R. H. Friend and F. Li, *Nature*, 2018, **563**, 536–540; (c) S. Kimura, A. Tanushi, T. Kusamoto, S. Kochi, T. Sato and H. Nishihara, *Chem. Sci.*, 2018, **9**, 1996–2007; (d) Q. Peng, A. Obolda, M. Zhang and F. Li, *Angew. Chem., Int. Ed.*, 2015, **54**, 7091–7095.

8 (a) C. M. Wehrmann, R. T. Charlton and M. S. Chen, *J. Am. Chem. Soc.*, 2019, **141**, 3240–3248; (b) T. Kubo, *Chem. Rec.*, 2015, **15**, 218–232; (c) S. K. Pal, M. E. Itkis, R. W. Reed, R. T. Oakley and R. C. Haddon, *Science*, 2005, **309**, 281–284.

9 M. Imran, C. M. Wehrmann and M. S. Chen, *J. Am. Chem. Soc.*, 2020, **142**, 38–43.

10 T. Itoh, *Chem. Rev.*, 2012, **112**, 4541–4568.

11 (a) P. R. Ogilby, *Chem. Soc. Rev.*, 2010, **39**, 3181–3209; (b) A. Greer, *Acc. Chem. Res.*, 2006, **39**, 797–804; (c) M. C. DeRosa and R. J. Crutchley, *Coord. Chem. Rev.*, 2002, **233–234**, 351–371.

12 M. J. Frisch, G. W. Trucks, H. B. Schlegel, G. E. Scuseria, M. A. Robb, J. R. Cheeseman, G. Scalmani, V. Barone, G. A. Petersson, H. Nakatsuji, X. Li, M. Caricato, A. Marenich, J. Bloino, B. G. Janesko, R. Gomperts, B. Mennucci, H. P. Hratchian, J. V. Ortiz, A. F. Izmaylov, J. L. Sonnenberg, D. Williams-Young, F. Ding, F. Lipparini, F. Egidi, J. Goings, B. Peng, A. Petrone, T. Henderson, D. Ranasinghe, V. G. Zakrzewski, J. Gao, N. Rega, G. Zheng, W. Liang, M. Hada, M. Ehara, K. Toyota, R. Fukuda, J. Hasegawa, M. Ishida, T. Nakajima, Y. Honda, O. Kitao, H. Nakai, T. Vreven, K. Throssell, J. A. Montgomery Jr, J. E. Peralta, F. Ogliaro, M. Bearpark, J. J. Heyd, E. Brothers, K. N. Kudin, V. N. Staroverov, T. Keith, R. Kobayashi, J. Normand, K. Raghavachari, A. Rendell, J. C. Burant, S. S. Iyengar, J. Tomasi, M. Cossi, J. M. Millam, M. Klene, C. Adamo, R. Cammi, J. W. Ochterski, R. L. Martin, K. Morokuma, O. Farkas, J. B. Foresman and D. J. Fox, *Gaussian 09, Revision D.01*, Gaussian, Inc., Wallingford CT, 2016.

13 (a) S. Grimme, J. Antony, S. Ehrlich and H. Krieg, *J. Chem. Phys.*, 2010, **132**, 154104; (b) G. Scalmani and M. J. Frisch, *J. Chem. Phys.*, 2010, **132**, 114110.

14 (a) N. S. Hill and M. L. Coote, *Annu. Rep. Comput. Chem.*, 2019, **15**, 203–285; (b) W. Liu and Y. Xiao, *Chem. Soc. Rev.*, 2018, **47**, 4481–4509; (c) T. W. Schmidt, *Int. Rev. Phys. Chem.*, 2016, **35**, 209–242; (d) S. Hirata, T. J. Lee and M. Head-Gordon, *J. Chem. Phys.*, 1999, **111**, 8904.

15 (a) B. Suo, K. Shen, Z. Li and W. Liu, *J. Phys. Chem. A*, 2017, **121**, 3929–3942; (b) S. Grimme and M. Parac, *ChemPhysChem*, 2003, **3**, 292–295; (c) D. J. Tozer, R. D. Amos, N. C. Handy, B. O. Roos and L. Serrano-Andres, *Mol. Phys.*, 1999, **97**, 859–868.

16 A. Dreuw and M. Head-Gordon, *Chem. Rev.*, 2005, **105**, 4009–4037.

17 C. He, Z. Li, Y. Lei, W. Zou and B. Suo, *J. Phys. Chem. Lett.*, 2019, **10**, 574–580.

18 M. Matsumoto, I. Antol and M. Abe, *Molecules*, 2019, **24**, 209.

19 (a) E. R. Darzi and R. Jasti, *Chem. Soc. Rev.*, 2015, **44**, 6401–6410; (b) Y. Segawa, A. Fukazawa, S. Matsuura, H. Omachi, S. Yamaguchi, S. Irle and K. Itami, *Org. Biomol. Chem.*, 2012, **10**, 5979–5984; (c) T. Iwamoto, Y. Watanabe, Y. Sakamoto, T. Suzuki and S. Yamago, *J. Am. Chem. Soc.*, 2011, **133**, 8354–8361.